

# Quantification of non-Markovian effects in the Fenna-Matthews-Olson complex

C. A. Mujica-Martinez, P. Nalbach, and M. Thorwart

*I. Institut für Theoretische Physik, Universität Hamburg, Jungiusstraße 9, 20355 Hamburg, Germany*

(Received 15 August 2013; published 19 December 2013)

The excitation energy transfer dynamics in the Fenna-Matthews-Olson complex is quantified in terms of a non-Markovianity measure based on the time evolution of the trace distance of two quantum states. We use a system description derived from experiments and different environmental fluctuation spectral functions, which are obtained either from experimental data or from molecular dynamics simulations. These exhibit, in all cases, a nontrivial structure with several peaks attributed to vibrational modes of the pigment-protein complex. Such a structured environmental spectrum can, in principle, give rise to strong non-Markovian effects. We present numerically exact real-time path-integral calculations for the transfer dynamics and find, in all cases, a monotonic decrease of the trace distance with increasing time which renders a Markovian description valid.

DOI: [10.1103/PhysRevE.88.062719](https://doi.org/10.1103/PhysRevE.88.062719)

PACS number(s): 87.15.H-, 03.65.Yz, 03.65.Ud, 03.65.Ta

## I. INTRODUCTION

In photosynthesis, the energy of solar photons is converted into chemical energy, which is used by the plants for their physiological processes. The photon absorption occurs at (antenna) pigment-protein complexes, generating an exciton. This is transferred toward the reaction center, where charge separation occurs. One of the most extensively studied pigment-protein complexes is the Fenna-Matthews-Olson (FMO) complex. It is a small water-soluble protein unique to green sulfur bacteria [1] and responsible for passing the excitation energy from the chlorosome to the photosynthetic reaction center.

Recent experimental studies using two-dimensional electronic spectroscopy [2,3] on photosynthetic molecules (in particular the FMO complex) have revealed long-lasting coherent oscillations of the nondiagonal peaks at cryogenic [4–6] and, surprisingly, also at room temperature [7–9]. This has led to an increasing interest in elucidating the role played by quantum coherence on the energy transfer dynamics of these systems [10–21]. In order to explain these long-lasting coherences, several models have been proposed, e.g., nonadiabatic vibrational-electronic mixing [20], vibrational coherences [15,19], and vibronic excitons [16,21].

Because of the large amount of atoms constituting the pigment-protein complexes, a full microscopic description is cumbersome. Therefore, the electronic states of these complexes are treated within an open quantum system approach [22]. In this approach, the dynamics of a given quantum system of interest is subject to the coupling to thermal fluctuations generated by an environment held at temperature  $T$ . Commonly, in most physical situations, Gaussian fluctuations prevail and thus can be described in a model based on a collection of quantum mechanical harmonic oscillators. The statistical properties of the quantum mechanical (operator-valued) fluctuating forces  $\xi(t)$  then crucially determine the relaxation and decoherence features of the quantum system. A straightforward assumption is that the fluctuations at a certain instant of time do not depend on their previous history and thus are uncorrelated over time. A Markovian approximation can be made and the resulting time evolution becomes local in time, rendering the solution of the underlying equations of motion rather simple. To judge the viability of the Markov approximation, the autocorrelation function of the fluctuations has to be

considered. The properties of the environmental harmonic oscillators, i.e., their masses  $m_k$ , frequencies  $\omega_k$ , and the coupling constants  $\kappa_k$ , can be collected in the spectral density  $G(\omega) = \sum_k \kappa_k^2 / (2m_k \omega_k) \delta(\omega - \omega_k)$  [22]. Then, the temporal correlation properties of the fluctuations are given by the bath autocorrelation function [22]

$$L(t) = \langle \xi(t) \xi(0) \rangle_T = \int_0^\infty d\omega G(\omega) \left[ \coth \frac{\hbar\omega}{2k_B T} \cos \omega t - i \sin \omega t \right], \quad (1)$$

where  $\hbar$  is the Planck constant divided by  $2\pi$  and  $k_B$  is the Boltzmann constant. Thus, the fluctuations are composed of harmonic modes with frequency  $\omega$  at temperature  $T$ , and each mode contributes with a spectral weight given by  $G(\omega)$ .

For many condensed matter systems, the typical situation [22] corresponds to a bath with a smooth structureless spectral density in the form of an ohmic spectral density  $G(\omega) \propto \omega \exp(-\omega/\omega_c)$  with a cutoff frequency  $\omega_c$ , which is chosen to be the largest frequency scale in the problem. The resulting autocorrelation function  $L(t)$  for large  $\omega_c$  is strongly peaked at short times and can safely be approximated by a  $\delta$  function. This implies that the environmental fluctuations evolve on the shortest time scale characterized by  $\omega_c^{-1}$ , describing a fast bath, where the memory effects are rather instantaneously lost or simply do not exist [23].

In extended bulk condensed matter systems, ohmic environments are ubiquitous, but nonohmic and highly structured environmental spectral densities arise in finite size systems, such as, for instance, photoactive molecular complexes. There, after the formation of an exciton, its quantum dynamics is subject to fluctuating electric fields at the exciton position. The fluctuations are created by a continuous distribution of fluctuating polarization modes generated either by a polar solvent or by a surrounding protein. The underlying spectral density can be obtained from experimental data (see, for instance, Ref. [24] for the fluctuational spectrum in the FMO molecular complex), or from numerical simulations, such as molecular dynamics calculations [25], or from theoretical modeling of the dielectric functions  $\epsilon(\omega)$ , for instance, in the Onsager continuum model of solvation [26]. These fluctuations are reminiscent of phonons in a crystal.

However, the molecular complexes typically have distinct molecular vibrational modes at particular frequencies. For instance, up to 30 different discrete vibrational molecular modes have been identified experimentally in the FMO complex [24]. One can include such sharp molecular modes in the environmental spectral density via  $\delta$  peaks at the mode frequencies. The consequence for the correlation properties is immediately clear if we consider for the moment such a single vibrational mode at frequency  $\Omega > 0$  by  $G_\Omega(\omega) \propto \delta(\omega - \Omega)$ . For temperatures  $k_B T \ll \hbar\Omega$ , pertinent oscillatory correlations are generated according to  $L(t) \propto e^{-i\Omega t}$ , which follows from Eq. (1). If we associate a finite linewidth  $\gamma_0$  to this vibrational mode, the oscillatory correlations decay exponentially with time according to  $L(t) \propto e^{-i\Omega t - \gamma_0 t}$  [27]. When these vibrational lifetimes are on the order of the system time scale, all bath-induced memory effects live on a comparable time scale and a Markovian approximation no longer can be made *a priori* for such a highly structured environmental spectrum [27]. Such vibrational degrees of freedom are common to large molecular complexes. For instance, a typical environmental fluctuation spectral function of the FMO complex is obtained either from experimental data [24] or from molecular dynamics simulations [25,28]. They are highly structured with many prominent vibrational peaks which induce a complicated pattern of several vibrational oscillatory correlations with long lifetime.

In order to describe the dynamics of an open quantum system beyond a Markovian approximation, few numerically exact approaches are available. These all need substantial computer power [29], which limits their application to rather small molecular complexes such as, for example, the FMO complex. Investigations of the energy transfer efficiency through the FMO complex typically employ Markovian master equations (see, for example, [30,31]), although it has been shown that a weak-coupling Markovian approach fails [12,32,33], the reason being [12] that multiphonon processes are neglected. The question, however, of whether or not the exact dynamics is Markovian has not been studied so far. In the case that the dynamics is Markovian, a weak-coupling lowest order Born approximation can still not be used to determine the Redfield rate tensor [12,32,33]. However, importantly, a Markovian quantum master equation could still be used to discuss the dynamics, for example, of the transfer efficiency [30,31], if the rate tensor is either treated as an effective fit parameter or obtained from some more advanced

theory. In turn, this would be beneficial since it would allow us to investigate larger molecular complexes.

To quantify how much the resulting dynamics is non-Markovian and, therefore, how reliable a Markovian approximation could be, several measures of the non-Markovianity have been recently proposed [34–36] based on different mathematical and physical concepts. For example, the non-Markovianity measure in Ref. [36] is rooted in the mathematical property of the dynamical map that generates the quantum time evolution, i.e., the deviation from divisibility of the trace-preserving completely positive map. On the other hand, the non-Markovianity measure in Ref. [35] is based on the physical features of the system-bath interaction in terms of information backflow from the environment to the system, which has been experimentally measured [37,38]. We therefore use this last measure to quantify non-Markovian effects during the excitation energy transfer dynamics of the FMO complex in the presence of discrete vibrational modes.

In the next section, we indicate how the FMO complex is modeled and show explicitly the different environmental fluctuation spectral functions used in this work. We then briefly present the non-Markovianity measure we used in Sec. III. The excitation energy transfer dynamics is simulated by using the numerically exact quasiadiabatic propagator path integral (QUAPI) method and quantified in terms of the trace distance in Sec. IV. Finally, concluding remarks are provided in Sec. V.

## II. FMO MODEL

The FMO protein consists of three identical and weakly interacting subunits, each of which contains eight bacteriochlorophyll *a* (BChl*a*) molecular sites [1,39]. The eighth pigment was recently resolved [40,41], but it is only very weakly coupled to the other BChls in the subunit and thus irrelevant for the present investigation. Each pigment is described as a two-level system restricting the consideration to the ground and first excited state. The different times scales of fast exciton transfer ( $\sim 1$  ps) as compared to the slow recombination ( $\sim 1$  ns) allow us to reduce the problem further and to describe the exciton dynamics within the single excitation subspace. The numerically determined site energies and dipolar couplings result in the Hamiltonian [42]

$$H_{\text{FMO}} = \begin{pmatrix} 240 & -87.7 & 5.5 & -5.9 & 6.7 & -13.7 & -9.9 \\ & 315 & 30.8 & 8.2 & 0.7 & 11.8 & 4.3 \\ & & 0 & -53.5 & -2.2 & -9.6 & 6.0 \\ & & & 130 & -70.7 & -17.0 & -63.3 \\ & & & & 285 & 81.1 & -1.3 \\ & & & & & 435 & 39.7 \\ & & & & & & 245 \end{pmatrix} \quad (2)$$

in units of  $\text{cm}^{-1}$  in the site representation for *Chlorobium tepidum*, with BChl 3 defined as the site with the lowest energy [39].

The vibrational pigment-protein-solvent environment induces thermal fluctuations on the excitation transfer dynamics. We model them by employing an open system approach

[22,43] in terms of the total Hamiltonian

$$H = H_{\text{FMO}} + \sum_{j=1}^7 |j\rangle\langle j| \sum_k \kappa_k^{(j)} q_{j,k} + \sum_{j=1}^7 \frac{1}{2} \sum_k (p_{j,k}^2 + \omega_{j,k}^2 q_{j,k}^2), \quad (3)$$

with momenta  $p_{j,k}$ , displacement  $q_{j,k}$ , frequency  $\omega_{j,k}$ , and coupling  $\kappa_k^{(j)}$  of the environmental vibrations at site  $j$ . The fluctuations at different BChl sites are assumed to be identical but spatially uncorrelated [14].

Recent reports [16,19,44,45] indicate that vibrational degrees of freedom close to resonance to exciton transitions may be responsible for the long-lived oscillatory features in the two-dimensional electronic spectra of the FMO complex [5,7]. Therein, specific vibrational modes are treated as part of the system and thus on an equal footing as the exciton states. We note that, within the open system approach used here, the environment is typically assumed to be in thermal equilibrium, thus allowing a study of the influence of quantum and thermal equilibrium fluctuations on the system. By including specific vibrational modes with a substantial coupling to the system into the environmental spectrum one assumes, consequently, that the thermalization time scale of these modes are much shorter than any system time scale. This does not exclude non-Markovian dynamics of the system but only nonequilibrium fluctuations of the vibrational modes.

The environmental influence on the system dynamics is fully characterized by the spectral density function  $G(\omega) = \sum_{j,k} (|\kappa_k^{(j)}|^2 / 2\omega_{j,k}) \delta(\omega - \omega_{j,k})$  [22]. The environmental spectral density is not easily experimentally accessible and, likewise, various parametrizations have been obtained based on different approaches. Since, *a priori*, it is unclear whether they result in the same non-Markovianity, we study three different spectral densities known in the literature. Aghtar *et al.* [25] have obtained a spectral density from molecular dynamics simulations of the FMO complex in specific solvent environments. Adolphs and Renger [42] as well as Kreisbeck, Kramer, and co-workers [46,47] extract a spectral density from the results of temperature-dependent fluorescence line-narrowing measurements by Wendling *et al.* [24], but eventually they obtain different functions. Adolphs and Renger describe the phonon background based on data available for the B777-complexes [48] and then subsequently add a single intramolecular vibrational mode in the form of a Dirac-delta peak, which is believed to be the most relevant mode. In contrast, Kreisbeck and Kramer are forced to parametrize the spectral density functions as a sum of shifted Drude-Lorentz peaks due to the hierarchy equation of motion approach used to determine the dynamics. We will study all three cases separately below.

#### A. Fluctuational spectrum of Adolphs and Renger

Adolphs and Renger [42] give a closed expression for the spectral density based on two contributions: (i) a broad continuous low-frequency part  $S_0 g_0(\omega)$ , which originates in the phonon-like protein vibrations and contributes with the Huang-Rhys factor  $S_0$ , and (ii) a single effective vibrational mode  $S_H \delta(\omega - \omega_H)$  of the pigments with Huang-Rhys factor

$S_H$ . The total spectral density is given as

$$G(\omega) = \omega^2 S_0 g_0(\omega) + \omega^2 S_H \delta(\omega - \omega_H). \quad (4)$$

If one assumes that the local modulation of pigment transition energies by the protein environment is a global quantity that does not differ much between the specific environment of the pigments [42], the low-frequency function  $g_0(\omega)$  has the same form as the spectral density that was originally extracted from 1.6 K fluorescence line-narrowing spectra of B777-complexes [48]. In particular, it has the form

$$g_0(\omega) = (6.105 \times 10^{-5}) \frac{\omega^3}{\omega_1^4} \exp\left[-\sqrt{\frac{\omega}{\omega_1}}\right] + (3.8156 \times 10^{-5}) \frac{\omega^3}{\omega_2^4} \exp\left[-\sqrt{\frac{\omega}{\omega_2}}\right], \quad (5)$$

with  $\omega_1 = 0.575 \text{ cm}^{-1}$  and  $\omega_2 = 2 \text{ cm}^{-1}$ . The Huang-Rhys factor of the protein-pigment coupling was estimated by Wendling *et al.* [24] from the temperature dependence of the absorption spectra to be  $S_0 \sim 0.5$  and yields a satisfactory agreement with the experimental data.

In addition, Adolphs and Renger have included an effective single vibrational mode of the pigments at frequency  $\omega_H = 180 \text{ cm}^{-1}$  with the Huang-Rhys factor  $S_H = 0.22$  [42]. Earlier, Wendling *et al.* [24], for instance, have identified up to 30 vibrational modes in their experimental data. They arrive at an overall Huang-Rhys factor of  $0.45 \pm 0.05$ , while they obtain a Huang-Rhys factor of 0.3 for the continuous phonon background. Out of this, Adolphs and Renger constructed an effective Huang-Rhys factor of the single vibrational mode at  $180 \text{ cm}^{-1}$  of  $S_H = 0.22$  by including all high-frequency vibrational modes into an effective single mode. The value of  $S_H = 0.22$  given by Adolphs and Renger appears to be somewhat large, which is due to the effective description [42]. In more detail, the effective mode at  $180 \text{ cm}^{-1}$  in fact consists of three strongly overlapping vibrational modes at 173, 185, and  $195 \text{ cm}^{-1}$ . Following Wendling *et al.* [24], we may combine the weight of the three modes around  $180 \text{ cm}^{-1}$  out of the 30 modes to an effective Huang-Rhys factor of  $S_H = 0.027$ . Likewise, in a related work on the vibronic fine structure of the light-harvesting complex II of green plants [49], also up to 48 vibrational modes were found with considerably smaller Huang-Rhys factors. Hence, for the single effective vibrational mode constructed by Adolphs and Renger [42], all weight is concentrated at this mode while, in reality, the spectral weight is spread over many channels. Since we are interested in the non-Markovian properties, they would be weaker for smaller Huang-Rhys factors and, thus, we consider the case of the largest Huang-Rhys factor of  $S_H = 0.22$  in the following.

Under realistic physiological conditions, the unphysical  $\delta$  peak should be broadened since the protein is embedded in water, which, as a polar solvent, gives rise to an additional weak ohmic damping of the protein vibrations [14]. We assume that the broadening has a Lorentzian line shape with width  $\gamma$  in the form

$$\omega^2 S_H \delta(\omega - \omega_H) \rightarrow S_H \omega^2 \gamma \frac{\omega^2}{(\omega^2 - \omega_H^2)^2 + (\gamma \omega)^2}. \quad (6)$$

This specific form of the peak ensures that the Huang-Rhys factor  $S_H$  is kept constant when varying the width  $\gamma$ . In Fig. 1,

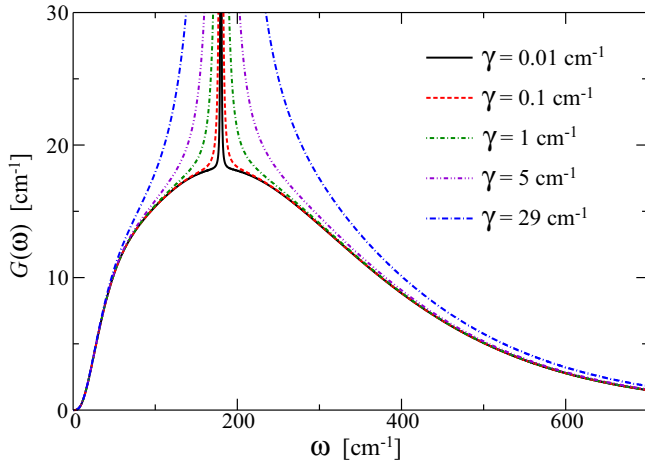


FIG. 1. (Color online) Spectral density function of Adolphs and Renger [Eq. (4)] for different Lorentzian peak widths  $\gamma$  centered at  $\omega_H = 180 \text{ cm}^{-1}$ .

we show the resulting spectral density function of Eq. (4) for several widths  $\gamma$ . Typically, peaked spectral functions result in strong non-Markovian dynamics [27,50]. However, in the present case the continuous background spectrum  $g_0(\omega)$  is rather large (see Fig. 1), which broadens the exciton transitions, leading to a weak dependence on the width  $\gamma$  and position  $\omega_H$  of the Lorentzian peak and washing out non-Markovian effects (see Sec. IV A).

The influence of vibrational modes on the system dynamics is relevant only when their energies are comparable to the energy difference between the exciton states [51]. The exciton states of the FMO complex are obtained by diagonalizing Eq. (2), with the squares of the eigenvector elements of the seven exciton states tabulated in Table I and schematically shown in Fig. 2.

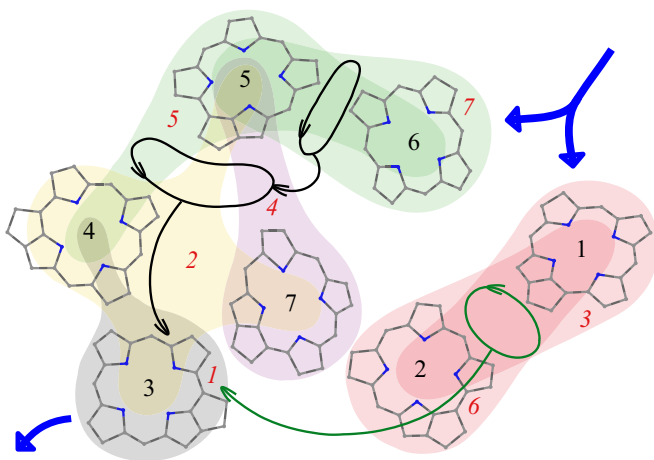


FIG. 2. (Color online) Structural arrangement of the seven BChl molecules (black numbers) in FMO (*Chl. tepidum*) [40,52] superposed with a schematic representation of the delocalization patterns of the different excitons (colored shading, italic red numbers). The exciton numeration is in ascending energy order. The two main excitation transfer routes are indicated by the green and black thin arrows. Entrance and exit sites are indicated by blue thick arrows.

Experimental results [39,53] indicate that BChls 1 and 6 are oriented toward the peripheral chlorosome antenna complex. Therefore, it is believed that these are the initially excited sites. In contrast, BChl 3 interacts with the cytoplasmic membrane, which embeds the reaction center. The orientation of this site and the fact that it has the lowest energy indicates that BChl 3 is the exit site. As indicated in Table I and Fig. 2, the lowest energy exciton 1 is almost completely localized at BChl 3, which is in agreement with this site being the energy sink toward the reaction center. The exciton pair 3 and 6 is mainly localized on BChls 1 and 2. These two BChls are the ones which are most strongly coupled in the Adolphs-Renger FMO Hamiltonian [Eq. (2)]. Meanwhile, the pair of excitons 5 and 7 is mainly localized on BChls 5 and 6, which is the second most strongly coupled BChl pair. By diagonalizing the FMO Hamiltonian in Eq. (2), we found that the energy difference between excitons 3 and 6 and between excitons 5 and 7 is  $190.8$  and  $211.0 \text{ cm}^{-1}$ , respectively. Due to the orientation of BChls 1 and 6, it is expected that these specific excitons play a relevant role on the excitation energy transfer dynamics, in particular, since their energy difference is close to that of the localized vibrational mode at  $180 \text{ cm}^{-1}$ .

In order to evaluate the influence of a localized vibrational mode in resonance with exciton transitions, we calculate the dynamics when the Lorentzian peak is exactly in resonance with the energy difference between excitons 3 and 6 and between excitons 5 and 7, which corresponds to  $\omega_H$  values of  $190.8$  and  $211.0 \text{ cm}^{-1}$ , respectively. We also examine the dynamics in the case where no localized vibration exist, i.e., no peak ( $\gamma = 0$ ). The resulting spectral density functions for  $\omega_H$  in resonance with excitonic energy differences and with no localized vibrational mode are shown in Fig. 3.

### B. Fluctuational spectrum of Kreisbeck and Kramer

The vibronic component of the experimentally determined fluctuational spectrum of the FMO complex [24] was parametrized by Kreisbeck, Kramer, and co-workers [46,47]

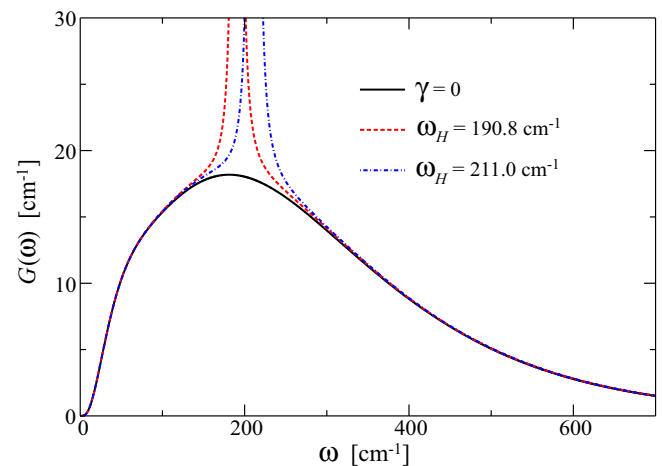


FIG. 3. (Color online) Spectral density function of Adolphs and Renger [Eq. (4)] with no localized vibrational mode (solid black line) and for  $\omega_H$  in resonance with excitonic energy differences:  $\omega_H = 190.8 \text{ cm}^{-1}$  (dashed red line) and  $\omega_H = 211.0 \text{ cm}^{-1}$  (dash-dotted blue line).  $\gamma = 1 \text{ cm}^{-1}$  in both cases.

TABLE I. Square of the eigenvector elements of the FMO Hamiltonian [Eq. (2)] in the exciton representation with exciton numeration in ascending energy order. The negative sign (−) indicates that the corresponding eigenvector element is negative and the bold numbers indicate the predominant site contribution to the excitonic state.

	BChl 1	BChl 2	BChl 3	BChl 4	BChl 5	BChl 6	BChl 7
Exciton 1	(−)0.0019	(−)0.0108	<b>0.8255</b>	<b>0.1485</b>	0.0085	0.0002	0.0047
Exciton 2	0.0066	0.0029	(−) <b>0.1418</b>	<b>0.5923</b>	<b>0.1057</b>	(−)0.0086	<b>0.1420</b>
Exciton 3	<b>0.6934</b>	<b>0.2745</b>	0.0140	(−)0.0005	(−)0.0137	0.0034	0.0006
Exciton 4	(−)0.0011	(−)0.0140	0.0016	(−)0.0256	(−) <b>0.2562</b>	0.0014	<b>0.7002</b>
Exciton 5	0.0002	0.0138	0.0144	(−) <b>0.2048</b>	<b>0.4314</b>	(−) <b>0.2181</b>	0.1174
Exciton 6	<b>0.2909</b>	(−) <b>0.6741</b>	(−)0.0027	(−)0.0053	0.0226	0.0040	(−)0.0003
Exciton 7	0.0059	(−)0.0099	(−)0.0000	0.0231	(−) <b>0.1618</b>	(−) <b>0.7644</b>	(−)0.0348

using the Meier-Tannor decomposition [54] to represent general spectral density functions as a sum of shifted Drude-Lorentz peaks. The resulting spectral density function for the FMO complex has the form

$$G_n(\omega) = \sum_{k=1}^n \left[ \frac{v_k \lambda_k \omega}{v_k^2 + (\omega + \Omega_k)^2} + \frac{v_k \lambda_k \omega}{v_k^2 + (\omega - \Omega_k)^2} \right]. \quad (7)$$

Figure 4 shows the spectral density function in Eq. (7) with the corresponding parameters listed in Table II. The experimental spectral density is well approximated by the sum of 11 shifted Drude-Lorentz peaks [ $n = 11$  in Eq. (7)], reproducing the low-frequency portion and taking into account all the strongly coupled vibronic modes, which are visible as peaks in the spectral density function. An alternative parametrization with only three peaks [ $n = 3$  in Eq. (7)] is also given.

### C. Fluctuational spectrum of Aghtar *et al.*

As a third case, Aghtar *et al.* [25] have calculated the spectral density function for the FMO complex from molecular dynamics simulations. Their procedure [28], which has been also used in other photosynthetic systems such as the light-harvesting II complex [55], consists in ground-state energy minimizations at different temperatures and normal pressure, i.e., molecular dynamics simulations. The effects

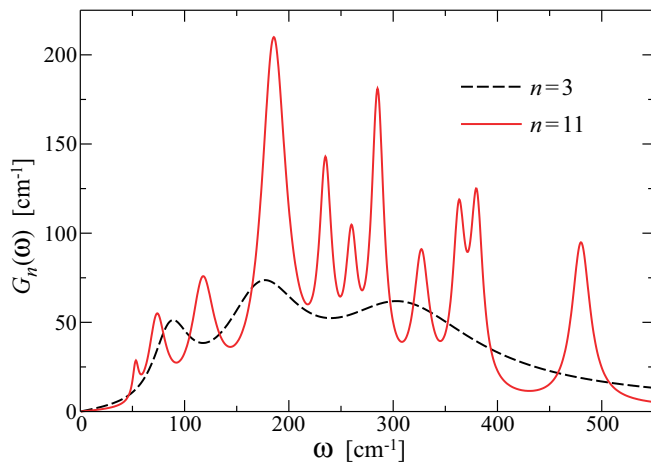


FIG. 4. (Color online) Spectral density function of Kreisbeck and Kramer for the FMO complex in the form of a sum of shifted Drude-Lorentz peaks [Eq. (7)] with the parameters listed in Table II.

of thermal fluctuations on the energy transfer dynamics and optical properties are accounted for by quantum chemistry calculations of the excitation energies and the electronic couplings along the molecular dynamics trajectories. For this, they use Zerner's intermediate neglect of differential overlap method with parameters for spectroscopic properties together with the configuration interaction scheme using single excitations only (ZINDO/S-CIS). With this they calculate the distribution of site energies for the individual BChls which are used to determine their spatial and temporal correlations. The time-dependent bath correlation function  $C_j(t)$  relates to the spectral density function  $G_j(\omega)$  of site  $j$  through

$$G_j(\omega) = \frac{2}{\pi \hbar} \tanh\left(\frac{\hbar\omega}{2k_B T}\right) \int_0^\infty dt C_j(t) \cos(\omega t). \quad (8)$$

The spectral density function  $G_j(\omega)$  describes the frequency-dependent coupling of BChl  $j$  to the thermal environment [25]. Molecular dynamics simulations allow one to include the microscopic description of the solvent environment used in the experimental measurements. Here, two specific cases are considered: water as a solvent at 300 K and a glycerol:water (65:35) mixture as a solvent at 310 K. The resulting site-dependent spectral density functions  $G_j(\omega)$  are shown in Fig. 5.

### III. MEASURE OF THE NON-MARKOVIANITY

In an open quantum system, the evolution of any two initial states  $\rho_{1,2}(0)$  is given by a family of trace-preserving and completely positive quantum dynamical maps  $\Phi(t,0)$  such that  $\rho_{1,2}(t) = \Phi(t,0)\rho_{1,2}(0)$ . These two quantum states can be distinguished in terms of the trace distance, which provides a metric in the space of physical states [56]. The dynamical change of the distinguishability of the states of an open quantum system can be interpreted in terms of information exchange between the system and its environment [56]. In a Markovian process, there is an infinitesimally small correlation time between the system and environment dynamics, which leads to a monotonic flow of information from the system to the environment. However, in a non-Markovian process the long-lived correlations may generate a backflow of information from the environment to the system and memory effects can then occur. In order to quantify the degree of non-Markovianity during the quantum evolution, several non-Markovianity measurements have been proposed. The one used here is based on physical features of the system-bath interaction, where the

TABLE II. Parameters of the spectral density function [Eq. (7)] derived by Kreisbeck and Kramer [46].  $\Omega_k$  and  $\lambda_k$  are given in units of  $\text{cm}^{-1}$  and  $\nu_k^{-1}$  is given in units of femtoseconds.

3 peaks	$\Omega_k$	85	170	300								
	$\nu_k^{-1}$	250	120	65								
	$\lambda_k$	10	15	13								
11 peaks	$\Omega_k$	53	73	117	185	235	260	285	327	363	380	480
	$\nu_k^{-1}$	1600	550	400	370	750	800	750	600	750	750	500
	$\lambda_k$	1.2	6.4	7.4	15.6	3.4	1.8	4	2	1.8	1.9	2

backflow of information from the environment to the system is quantified [35,57]. Other measurements, such as that proposed in Ref. [36], are based on the mathematical properties of the dynamical map that generates the quantum evolution. In general, these measures yield different results [58–62]. However, any process that is non-Markovian according to Ref. [35] is also non-Markovian according to Ref. [36], while the converse is not always true. The reason for this is that the conditions for information backflow are much more rigorous than that for indivisibility. Therefore, information backflow causes the indivisibility of the dynamics, but the reverse is not always true [60–62].

The information exchange between the system and its environment can be quantified through the dynamics of the trace distance between a pair of quantum states  $\rho_1$  and  $\rho_2$  of the open system, which is defined as [63]

$$D(\rho_1, \rho_2) = \frac{1}{2} \text{tr} |\rho_1 - \rho_2|, \quad (9)$$

where  $|O| = \sqrt{O^\dagger O}$ . The trace distance can be interpreted as a measure of the distinguishability of states  $\rho_1$  and  $\rho_2$ , satisfying  $0 \leq D \leq 1$  [35]. For open quantum systems, the trace distance of the states  $\rho_{1,2}(t)$  [evolving under the dynamical map  $\Phi(t)$ ] is a monotonically decreasing function of time  $D(\Phi\rho_1, \Phi\rho_2) \leq D(\rho_1, \rho_2)$ , which means that the distinguishability of two states

always decreases. In general, under a Markovian evolution, any two initial states become less and less distinguishable as time increases. This can be interpreted as an unidirectional flow of information from the system to the environment, which continuously reduces the possibility of distinguishing the given states [35].

If the rate of change of the trace distance is defined as

$$\sigma(t, \rho_{1,2}(0)) = \frac{d}{dt} D(\rho_1(t), \rho_2(t)), \quad (10)$$

which depends on the specific initial states  $\rho_{1,2}(0)$ , a Markovian evolution implies that  $\sigma \leq 0$  for all quantum processes. Conversely, a process is said to be non-Markovian if it satisfies  $\sigma > 0$ . In the latter case, the distinguishability of the pair of states increases at certain times by backflow of information from the environment to the system. The non-Markovianity measure [of the quantum process  $\Phi(t)$ ] quantifies the total increase of the distinguishability over the whole time evolution, i.e., the *total* amount of information which flows from the environment back to the system:

$$\mathcal{N}(\Phi) = \max_{\rho_{1,2}(0)} \int_{\sigma > 0} \sigma(t, \rho_{1,2}(0)) dt, \quad (11)$$

where the time integration extends over all time intervals  $(a_i, b_i)$  in which  $\sigma > 0$ , and the maximum is taken over all pairs of initial states [35,57]. Therefore,  $\mathcal{N}(\Phi)$  represents a functional of the family of dynamical maps  $\Phi(t)$  describing the physical process [64].

The non-Markovianity measure  $\mathcal{N}(\Phi)$  has been used to quantify non-Markovian effects during the quantum evolution of driven systems [58], the spin-boson model [64], biomolecular dimers [65], molecular charge qubits [66], initially correlated system-bath models [67,68], and others [69–73]. Very recently,  $\mathcal{N}(\Phi)$  has been measured experimentally for the polarization states of photons acting as system states, coupled to the photon frequency modes acting as environmental states. Non-Markovian dynamics has been induced by controlling the initial state of the environment [37] or by modifying the interaction between the system and the environment [38]. These results demonstrate that this particular measure provides an experimentally accessible observable which quantifies memory effects [56].

#### IV. NON-MARKOVIAN EFFECTS IN THE FMO COMPLEX

Here, non-Markovian effects in the exciton dynamics of the FMO complex arising from the different models presented in Sec. II are examined. All these models include explicitly localized vibrational modes, which can, in principle, induce strong non-Markovian behavior [27,50]. However, only vibrational modes up to energies which are comparable to the largest energy difference between the exciton states are relevant [51].

In order to quantify the non-Markovianity of the quantum evolution via Eq. (11), the explicit system dynamics is needed. This is given by the time evolution of the reduced density matrix  $\rho(t)$ , which is obtained after tracing out the bath degrees of freedom. Here, the reduced density matrix is calculated by using the QUAPI scheme [74], which is a numerically exact iteration scheme that has been successfully applied to many

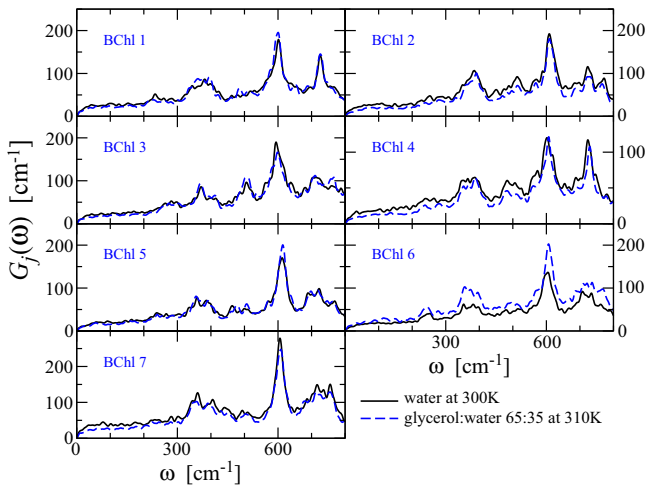


FIG. 5. (Color online) Site-dependent spectral density functions  $G_j(\omega)$  of Aghtar *et al.* for the FMO complex as determined from molecular dynamics simulations [25] with water as a solvent at 300 K (solid black line) and with a glycerol:water (65:35) mixture as a solvent at 310 K (dashed blue line).

problems of open quantum systems. In particular, it allows one to treat nearly arbitrary spectral functions at finite temperatures [14,23,66,75–77].

The non-Markovianity quantifier, Eq. (11), is calculated by a maximization procedure over all pairs of initial states [35,57]. It has been shown [59] that often this maximization can be removed without influencing the sensibility of the measure in finite-dimensional physical systems, which usually can only be prepared in specific initial states as is the case for the particular chromophores of photosynthetic complexes [14,65]. In the case of the FMO complex, these initial states are  $\rho_1(0) = \rho_{11}$  and  $\rho_2(0) = \rho_{66}$ , corresponding to the BChl 1 and BChl 6 sites (see Fig. 2), which are oriented toward the peripheral chlorosome [14,39,42,53].

Using this argument and Eq. (10) allow us to write the non-Markovianity measurement in the form

$$\mathcal{N} = \sum_i [D(\rho_1(b_i), \rho_2(b_i)) - D(\rho_1(a_i), \rho_2(a_i))], \quad (12)$$

with the sum running over all time intervals  $(a_i, b_i)$  during which the trace distance increases, thus integrating over all time spans of growing distinguishability.

#### A. Non-Markovianity in the Adolphs-Renger model

The evolution of the trace distance [Eq. (9)] for the spectral density function derived by Adolphs and Renger [Eq. (4)] in the absence of any localized vibrational mode ( $\gamma = 0$ ) is

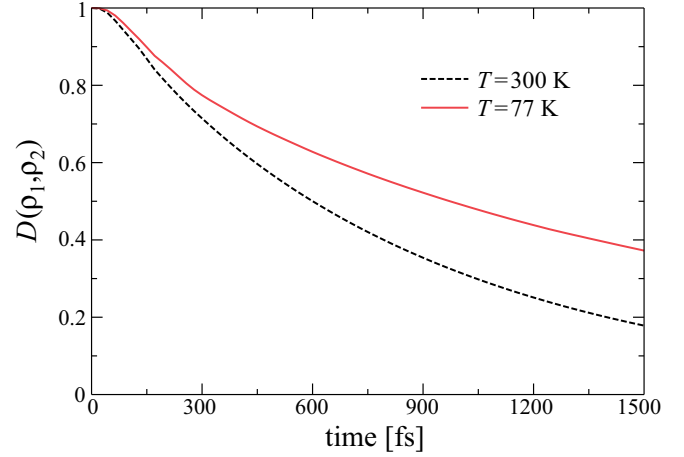


FIG. 6. (Color online) Time evolution of the trace distance [Eq. (9)] for the spectral density function derived by Adolphs and Renger [Eq. (4)] in the absence of any localized vibrational mode ( $\gamma = 0$ ).

shown in Fig. 6. We observe that the trace distance decays faster at higher temperatures and this decay is monotonic, indicating a unidirectional flow of information from the system to the environment, rendering the dynamics Markovian. The same kind of dynamics is observed for different positions  $\omega_H$  and widths  $\gamma$  of the Lorentzian peak in Eq. (4), as seen in Fig. 7. Because there is no time interval over which the trace

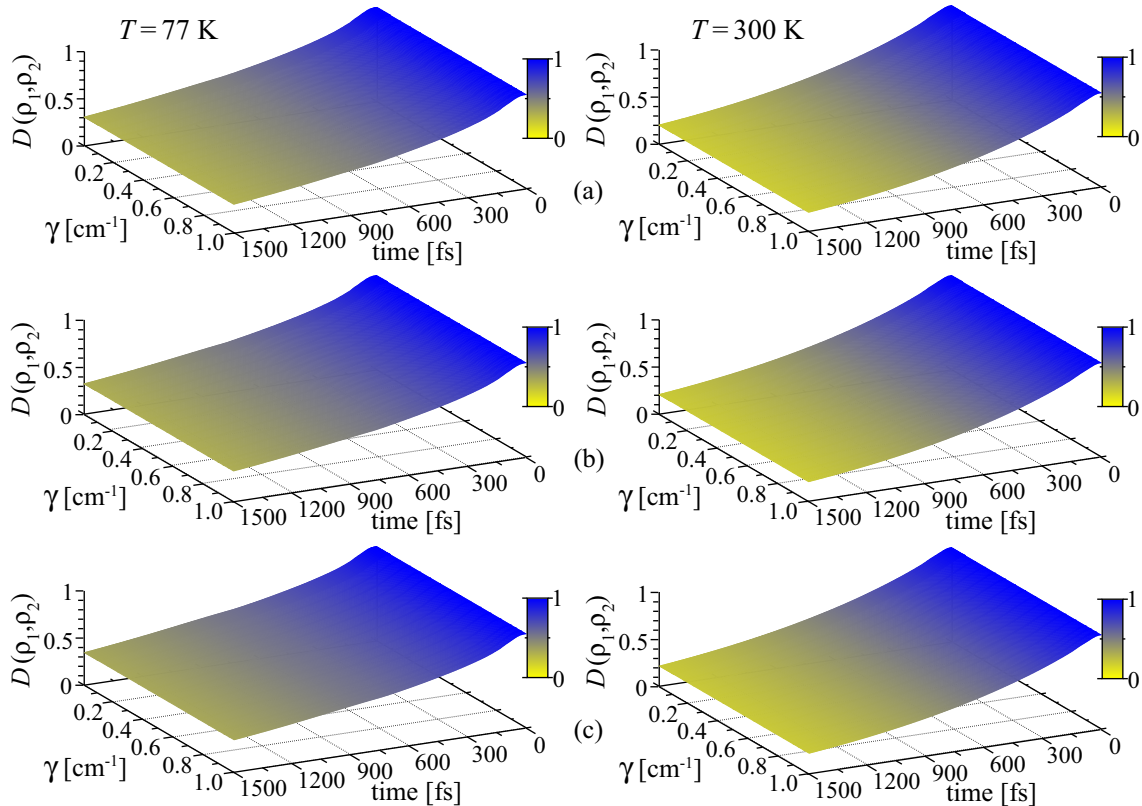


FIG. 7. (Color online) Time evolution of the trace distance [Eq. (9)] for the spectral density function derived by Adolphs and Renger [Eq. (4)] as a function of the width  $\gamma$  of the Lorentzian peak centered at (a) 180, (b) 190.8, and (c) 211.0  $\text{cm}^{-1}$ . Left and right columns correspond to temperatures of 77 and 300 K, respectively.

distance increases, we obtain  $\mathcal{N} = 0$  for all cases shown in Figs. 6 and 7. Our results indicate that the presence of a single localized vibrational mode in the bath spectral density does not induce any non-Markovian effect in the exciton dynamics of the FMO complex, even in the case when its frequency is exactly in resonance with exciton transitions. The broadening of the vibrational mode over a larger range of  $\gamma$  values (not shown) seems to have a negligible effect on the dynamics. This can be explained by observing that the continuous background spectrum  $g_0(\omega)$  in Eq. (4) is rather large (see Figs. 1 and 3), which results in linewidths for the exciton transitions already exceeding the width of the Lorentzian peak. In such a case, the Lorentzian peak becomes effectively *smearred out* and detailed results depend only weakly on its width  $\gamma$  and position  $\omega_H$ . This, in turn, would suppress any non-Markovian behavior too, as observed in Fig. 7.

### B. Non-Markovianity in the Kreisbeck-Kramer model

Figure 8 shows the time-dependent trace distance [Eq. (9)] for the spectral density derived by Kreisbeck and Kramer [Eq. (7)] with  $n = 3$  and  $n = 11$ . As before, at room temperature, we observe a faster monotonic decay of the trace distance as compared to the decay at cryogenic temperature. This decay is faster for  $n = 11$  than for  $n = 3$  due to the faster increase of the spectral weight of low-frequency modes in the former case (see Fig. 4). We obtain  $\mathcal{N} = 0$  for all the examined cases. These results allow us to conclude that, in spite of the role played by localized vibrational modes in the coherence times (not shown), they do not induce any non-Markovian effects in the exciton dynamics of the FMO complex.

### C. Non-Markovianity in the Aghtar *et al.* model

The evolution of the trace distance [Eq. (9)] for the spectral density function derived by Aghtar *et al.* [25] [Eq. (8)] from molecular dynamics simulations is shown in Fig. 9. In both cases, we observe a similar monotonic decay of the trace distance, which again indicates a Markovian dynamics

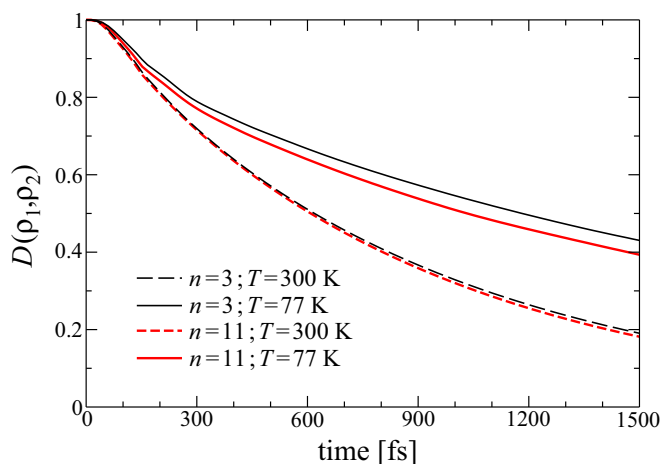


FIG. 8. (Color online) Time evolution of the trace distance [Eq. (9)] for the spectral density derived by Kreisbeck and Kramer [Eq. (7)] with  $n = 3$  (thin black lines) and  $n = 11$  (thick red lines) at 77 K (solid lines) and 300 K (dashed lines).

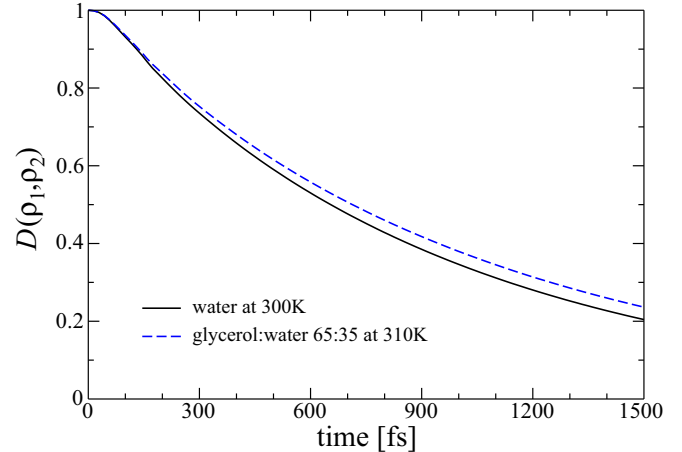


FIG. 9. (Color online) Time evolution of the trace distance [Eq. (9)] for the spectral density derived by Aghtar *et al.* [Eq. (8)] with water as a solvent at 300 K (solid black line) and with a glycerol:water (65:35) mixture as a solvent at 310 K (dashed blue line).

( $\mathcal{N} = 0$ ). The fact that the trace distance at 300 K decays faster than the case at 310 K is because the spectral weight at low frequencies for water as a solvent is larger than for the glycerol:water (65:35) mixture as a solvent (see Fig. 5). This allows us to rule out the possibility of non-Markovian effects arising from microscopic details of the polar environment.

## V. CONCLUSIONS

We have investigated possible non-Markovian effects in the excitation energy transfer dynamics of the FMO complex by using the numerically exact QUAPI scheme. The BChl system is described according to experimental results and the fluctuating pigment-protein-solvent environment is described by known spectral functions, which are obtained either from experimental data or from molecular dynamics simulations (Sec. II). All spectral density functions exhibit a nontrivial structure with several peaks attributed to vibrational modes of the pigment-protein complex, which are explicitly included as part of the environment. The spectral density functions derived by Adolphs and Renger [42], Eq. (4), and by Kreisbeck and Kramer [46], Eq. (7), include, respectively, a single and several localized vibrational modes. On the other hand, the site-dependent spectral density functions derived by Aghtar *et al.* [25], Eq. (8), include the specific microscopic details of the polar environment.

We have quantified the non-Markovian effects during the excitation transfer dynamics by means of a non-Markovianity measure based on the trace distance of two quantum states (Sec. IV). By evaluating the time evolution of the trace distance, we found that the presence of localized vibrational modes does not induce any non-Markovian effects in the exciton dynamics of the FMO complex. When considering a single mode in the bath spectral density (Sec. IV A), we found that neither its position nor its width induce any non-Markovian exciton dynamics, even in the case when its frequency is exactly in resonance with exciton transitions. These effects do not arise when several localized vibrational

modes are included (Sec. IV B) nor from the microscopic details of the polar environment (Sec. IV C).

Our results indicate that the excitation energy transfer dynamics of the FMO complex follows a Markovian dynamics. Similarly, it has been shown that the excitation energy transfer efficiency does not depend on the presence of non-Markovian effects [78]. The discrete vibrational modes within the environmental fluctuation spectra do not render the dynamics non-Markovian since the continuous phonon contribution of the fluctuation spectra results already in large linewidths for the exciton transitions. Hence, each exciton transition overlaps with the vibrational mode spectral peak, thus suppressing non-Markovian effects. The resulting Markovian dynamics is still not describable by weak system-bath coupling approaches

[12]. However, our results show that Markovian quantum master equations could be used to discuss the dynamics, or the transfer efficiency, if the rate tensor is either treated as an effective fitting parameter or obtained from some more involved theory approach. Our results therefore will help to considerably simplify the numerical effort in future investigations, and thus larger light-harvesting complexes will be treatable.

#### ACKNOWLEDGMENTS

We acknowledge financial support from the German Academic Exchange Service (DAAD) and from the DFG SFB 925.

- 
- [1] J. Overmann, in *Encyclopedia of Life Sciences* (Wiley, Chichester, 2001).
- [2] S. Mukamel, *Principles of Nonlinear Optics and Spectroscopy* (Oxford University Press, New York, 1995).
- [3] M. Cho, *Two-Dimensional Optical Spectroscopy* (CRC, Boca Raton, 2009).
- [4] T. Brixner, J. Stenger, H. M. Vaswani, M. Cho, R. E. Blankenship, and G. R. Fleming, *Nature (London)* **434**, 625 (2005).
- [5] G. S. Engel, T. R. Calhoun, E. L. Read, T.-K. Ahn, T. Mančal, Y.-C. Cheng, R. E. Blankenship, and G. R. Fleming, *Nature (London)* **446**, 782 (2007).
- [6] S. Westenhoff, D. Paleček, P. Edlund, P. Smith, and D. Zigmantas, *J. Am. Chem. Soc.* **134**, 16484 (2012).
- [7] G. Panitchayangkoon, D. Hayes, K. A. Fransted, J. R. Caram, E. Harel, J. Wen, R. E. Blankenship, and G. S. Engel, *Proc. Natl. Acad. Sci. USA* **107**, 12766 (2010).
- [8] E. Collini, C. Y. Wong, K. E. Wilk, P. M. G. Curmi, P. Brumer, and G. D. Scholes, *Nature (London)* **463**, 644 (2010).
- [9] E. Harel and G. S. Engel, *Proc. Natl. Acad. Sci. USA* **109**, 706 (2012).
- [10] M. Thorwart, J. Eckel, J. H. Reina, P. Nalbach, and S. Weiss, *Chem. Phys. Lett.* **478**, 234 (2009).
- [11] Y.-C. Cheng and G. R. Fleming, *Annu. Rev. Phys. Chem.* **60**, 241 (2009).
- [12] P. Nalbach and M. Thorwart, *J. Chem. Phys.* **132**, 194111 (2010).
- [13] P. Nalbach, J. Eckel, and M. Thorwart, *New J. Phys.* **12**, 065043 (2010).
- [14] P. Nalbach, D. Braun, and M. Thorwart, *Phys. Rev. E* **84**, 041926 (2011).
- [15] N. Christensson, F. Milota, J. Hauer, J. Sperling, O. Bixner, A. Nemeth, and H. F. Kauffmann, *J. Phys. Chem. B* **115**, 5383 (2011).
- [16] N. Christensson, H. F. Kauffmann, T. Pullerits, and T. Mančal, *J. Phys. Chem. B* **116**, 7449 (2012).
- [17] A. Ishizaki and G. R. Fleming, *Annu. Rev. Condens. Matter Phys.* **3**, 333 (2012).
- [18] N. Lambert, Y.-N. Chen, Y.-C. Cheng, C.-M. Li, G.-Y. Chen, and F. Nori, *Nat. Phys.* **9**, 10 (2013).
- [19] A. W. Chin, J. Prior, R. Rosenbach, F. Caycedo-Soler, S. F. Huelga, and M. B. Plenio, *Nat. Phys.* **9**, 113 (2013).
- [20] V. Tiwari, W. K. Peters, and D. M. Jonas, *Proc. Natl. Acad. Sci. USA* **110**, 1203 (2013).
- [21] A. Chenu, N. Christensson, H. F. Kauffmann, and T. Mančal, *Sci. Rep.* **3**, 2029 (2013).
- [22] U. Weiss, *Quantum Dissipative Systems*, 3rd ed. (World Scientific, Singapore, 2008).
- [23] J. Eckel, J. H. Reina, and M. Thorwart, *New J. Phys.* **11**, 085001 (2009).
- [24] M. Wendling, T. Pullerits, M. A. Przyjalowski, S. I. E. Vulto, T. J. Aartsma, R. van Grondelle, and H. van Amerongen, *J. Phys. Chem. B* **104**, 5825 (2000).
- [25] M. Aghtar, J. Strümpfer, C. Olbrich, K. Schulten, and U. Kleinekathöfer, *J. Phys. Chem. B* **117**, 7157 (2013).
- [26] A. Nitzan, *Chemical Dynamics in Condensed Phases: Relaxation, Transfer and Reactions in Condensed Molecular Systems* (Oxford University Press, Oxford, 2006).
- [27] M. Thorwart, E. Paladino, and M. Grifoni, *Chem. Phys.* **296**, 333 (2004).
- [28] C. Olbrich, J. Strümpfer, K. Schulten, and U. Kleinekathöfer, *J. Phys. Chem. Lett.* **2**, 1771 (2011).
- [29] P. Nalbach, A. Ishizaki, G. R. Fleming, and M. Thorwart, *New J. Phys.* **13**, 063040 (2011).
- [30] M. Mohseni, P. Rebentrost, S. Lloyd, and A. Aspuru-Guzik, *J. Chem. Phys.* **129**, 174106 (2008).
- [31] M. B. Plenio and S. F. Huelga, *New J. Phys.* **10**, 113019 (2008).
- [32] A. Ishizaki and G. R. Fleming, *J. Chem. Phys.* **130**, 234110 (2009).
- [33] A. Ishizaki and G. R. Fleming, *J. Chem. Phys.* **130**, 234111 (2009).
- [34] M. M. Wolf, J. Eisert, T. S. Cubitt, and J. I. Cirac, *Phys. Rev. Lett.* **101**, 150402 (2008).
- [35] H.-P. Breuer, E.-M. Laine, and J. Piilo, *Phys. Rev. Lett.* **103**, 210401 (2009).
- [36] A. Rivas, S. F. Huelga, and M. B. Plenio, *Phys. Rev. Lett.* **105**, 050403 (2010).
- [37] B.-H. Liu, L. Li, Y.-F. Huang, C.-F. Li, G.-C. Guo, E.-M. Laine, H.-P. Breuer, and J. Piilo, *Nat. Phys.* **7**, 931 (2011).
- [38] J.-S. Tang, C.-F. Li, Y.-L. Li, X.-B. Zou, G.-C. Guo, H.-P. Breuer, E.-M. Laine, and J. Piilo, *Europhys. Lett.* **97**, 10002 (2012).
- [39] M. T. W. Milder, B. Brüggemann, R. van Grondelle, and J. L. Herek, *Photosynth. Res.* **104**, 257 (2010).

- [40] D. E. Tronrud, J. Wen, L. Gay, and R. E. Blankenship, *Photosynth. Res.* **100**, 79 (2009).
- [41] M. Schmidt am Busch, F. Müh, M. El-Amine Madjet, and T. Renger, *J. Phys. Chem. Lett.* **2**, 93 (2011).
- [42] J. Adolphs and T. Renger, *Biophys. J.* **91**, 2778 (2006).
- [43] V. May and O. Kühn, *Charge and Energy Transfer Dynamics in Molecular Systems*, 3rd ed. (Wiley-VCH, Weinheim, 2011).
- [44] H. Hossein-Nejad, A. Olaya-Castro, and G. D. Scholes, *J. Chem. Phys.* **136**, 024112 (2012).
- [45] M. d. Rey, A. W. Chin, S. F. Huelga, and M. B. Plenio, *J. Phys. Chem. Lett.* **4**, 903 (2013).
- [46] C. Kreisbeck and T. Kramer, *J. Phys. Chem. Lett.* **3**, 2828 (2012).
- [47] C. Kreisbeck, T. Kramer, and A. Aspuru-Guzik, *J. Phys. Chem. B* **117**, 9380 (2013).
- [48] T. Renger and R. A. Marcus, *J. Chem. Phys.* **116**, 9997 (2002).
- [49] E. J. G. Peterman, T. Pullerits, R. van Grondelle, and H. van Amerongen, *J. Phys. Chem. B* **101**, 4448 (1997).
- [50] P. Haikka and S. Maniscalco, *Phys. Rev. A* **81**, 052103 (2010).
- [51] P. Nalbach and M. Thorwart, *J. Phys. B: At. Mol. Opt. Phys.* **45**, 154009 (2012).
- [52] Protein Data Bank file 3ENI.
- [53] J. Wen, H. Zhang, M. L. Gross, and R. E. Blankenship, *Proc. Natl. Acad. Sci. USA* **106**, 6134 (2009).
- [54] C. Meier and D. J. Tannor, *J. Chem. Phys.* **111**, 3365 (1999).
- [55] C. Olbrich and U. Kleinekathöfer, *J. Phys. Chem. B* **114**, 12427 (2010).
- [56] H.-P. Breuer, *J. Phys. B: At. Mol. Opt. Phys.* **45**, 154001 (2012).
- [57] E.-M. Laine, J. Piilo, and H.-P. Breuer, *Phys. Rev. A* **81**, 062115 (2010).
- [58] P. Haikka, J. D. Cresser, and S. Maniscalco, *Phys. Rev. A* **83**, 012112 (2011).
- [59] H.-S. Zeng, N. Tang, Y.-P. Zheng, and G.-Y. Wang, *Phys. Rev. A* **84**, 032118 (2011).
- [60] D. Chruściński, A. Kossakowski, and Á. Rivas, *Phys. Rev. A* **83**, 052128 (2011).
- [61] B. Vacchini, A. Smirne, E.-M. Laine, J. Piilo, and H.-P. Breuer, *New J. Phys.* **13**, 093004 (2011).
- [62] H. Zeng, N. Tang, Y. Zheng, and T. Xu, *Eur. Phys. J. D* **66**, 255 (2012).
- [63] M. A. Nielsen and I. L. Chuang, *Quantum Computation and Quantum Information*, 10th anniversary (ed.) (Cambridge University Press, Cambridge, 2010).
- [64] G. Clos and H.-P. Breuer, *Phys. Rev. A* **86**, 012115 (2012).
- [65] P. Reberntrost and A. Aspuru-Guzik, *J. Chem. Phys.* **134**, 101103 (2011).
- [66] C. A. Mujica-Martinez, P. Nalbach, and M. Thorwart, *Phys. Rev. Lett.* **111**, 016802 (2013).
- [67] A. Smirne, H.-P. Breuer, J. Piilo, and B. Vacchini, *Phys. Rev. A* **82**, 062114 (2010).
- [68] E.-M. Laine, J. Piilo, and H.-P. Breuer, *Europhys. Lett.* **92**, 60010 (2010).
- [69] T. J. G. Apollaro, C. Di Franco, F. Plastina, and M. Paternostro, *Phys. Rev. A* **83**, 032103 (2011).
- [70] J.-G. Li, J. Zou, and B. Shao, *Phys. Rev. A* **81**, 062124 (2010).
- [71] L. Mazzola, E.-M. Laine, H.-P. Breuer, S. Maniscalco, and J. Piilo, *Phys. Rev. A* **81**, 062120 (2010).
- [72] P. Haikka, S. McEndoo, G. De Chiara, G. M. Palma, and S. Maniscalco, *Phys. Rev. A* **84**, 031602 (2011).
- [73] E.-M. Laine, H.-P. Breuer, J. Piilo, C.-F. Li, and G.-C. Guo, *Phys. Rev. Lett.* **108**, 210402 (2012).
- [74] N. Makri and D. E. Makarov, *J. Chem. Phys.* **102**, 4600 (1995); **102**, 4611 (1995).
- [75] M. Thorwart, P. Reimann, P. Jung, and R. Fox, *Chem. Phys.* **235**, 61 (1998).
- [76] M. Thorwart, J. Eckel, and E. R. Mucciolo, *Phys. Rev. B* **72**, 235320 (2005).
- [77] P. Nalbach and M. Thorwart, *Phys. Rev. Lett.* **103**, 220401 (2009).
- [78] S. Jesenko and M. Žnidarič, *J. Chem. Phys.* **138**, 174103 (2013).